Journal of Telecommunication, Electronic and Computer Engineering
ISSN: 2180 – 1843 e-ISSN: 2289-8131 Vol. 16 No. 1
jtec.utem.edu.my
DOI: https://doi.org/10.54554/jtec.2024.16.01.003

New 7D and Memristor-Based 8D Chaotic Systems: Computer Modeling and Circuit Implementation

M. Kopp
Institute for Single Crystals, NAS Ukraine, Nauky Ave. 60, Kharkiv 61072, Ukraine
michaelkopp0165@gmail.com

Article Info

Article history:
Received Dec 17th, 2023
Revised Feb 21st, 2024
Accepted Mar 17th, 2024
Published Mar 31st, 2024

Index Terms:
Nonlinear Dynamic Systems
Chaotic Behavior
Memristor
Computer Simulation
Circuit Implementation

Abstract

The most pressing modern problem of using chaotic systems in practice is the development of multi-channel information encryption methods. To solve these problems, there is a need to develop multidimensional chaos generators. In this paper, novel multidimensional 7D and 8D hyperchaotic systems are presented. It details a technique for creating a 7D dynamic system derived from a pre-existing 6D dynamic system. Additionally, this paper outlines the development of an 8D nonlinear dynamic system utilizing a memristor. An examination of innovative 7D and 8D dynamic systems was conducted, focusing on the determination of Lyapunov exponents, the construction of bifurcation diagrams, and the identification of equilibrium points along with their corresponding stability conditions for each system. As a result of computer modeling of 7D and 8D hyperchaotic systems in MATLAB-Simulink and Labview, phase portraits of numerous strange attractors were obtained. Finally, using Multisim software, electronic circuits for new 7D and 8D chaos generators were built, which demonstrated similar behavior as in the MATLAB-Simulink and LabView models.

I. INTRODUCTION

For many years, the scientific community has dedicated its efforts to examining nonlinear dynamical systems. Despite being governed by fixed rules or equations and considered deterministic, these systems display intricate, unpredictable, and seemingly random patterns over time. This phenomenon, known as deterministic chaos, is gaining prominence for its application in addressing diverse engineering challenges, notably in designing telecommunication systems [1]-[3]. In this context, emphasis is placed on the physical representation of nonlinear dynamic equations achieved by employing electronic circuits to devise novel chaos generators.

One of the dynamic systems frequently investigated for its chaotic attributes is the Lorentz system [4], originally formulated to describe free convection in the atmosphere. Cuomo and Oppenheim [5] devised an electronic circuit to generate chaotic signals, utilizing the Lorentz equations as a foundation. Furthermore, the authors detailed a technique within [5] for secure information exchange. This method involved employing synchronized chaotic Lorentz systems implemented in both the transmitter and the receiver. Research [5] stimulated the development of electronic chaos generators based on various equations. The Kaplan-York dimension and Lyapunov exponents stand out as pivotal tools for characterizing the chaotic dynamics of a system [6]. In instances where multiple positive Lyapunov exponents are present, the system's dynamics showcase more intricate chaotic behavior, commonly referred to as hyperchaotic.

Typically, dynamic systems with dimensions exceeding three manifest hyperchaotic behavior. Numerous studies have delved into hyperchaotic systems, each introducing distinct dimensions and characteristics. Vaidyanathan et al. [7] introduced a novel 4D hyperchaotic system lacking equilibrium and explored the synchronization possibilities of this new system. Singh et al. [8] proposed a 5D hyperchaotic system featuring a stable equilibrium point. Their work demonstrated multistability and transient chaotic behavior in the proposed system. Alattas et al. [9] addressed the synchronization of 6D hyperchaotic systems using integral-type sliding mode control. They also presented an analog electronic circuit utilizing MultiSIM. Kopp et al. [10] developed computer models for a 6D chaotic dynamic system using MATLAB-Simulink and LabVIEW. They employed the NI MultiSim package for circuit implementation, proposing a secure communication scheme based on chaotic modulation. Laghmiri et al. [11] constructed two new 7D hyperchaotic systems and conducted a comprehensive study on the dynamics and synchronization of these systems. Kopp et al. [12] designed computer models for an 8D Lorentz-like chaotic dynamical system in Matlab-Simulink and LabView. They utilized the NI MultiSim package for chaos generator electronics and implemented the 8D hyperchaotic system on the Arduino Uno board. Zhu et al. [13] introduced a nine-dimensional, eight-order chaotic system along with its corresponding circuit implementation. Mahmud et al. [14] presented a complex nonlinear hyperchaotic model, describing a nine-dimensional chaotic Lorentz system with

quaternion variables. Jianliang et al. [15] proposed a ten-dimensional chaotic system of the ninth order, implementing an electronic circuit for a chaos generator. Benkouider et al. [16] introduced an intricate 10D hyperchaotic system of substantial complexity. Through the active control method, they successfully demonstrated synchronization between a set of three chaotic systems and the 10D hyperchaotic system. Notably, despite the intricate dynamics inherent in the new 10D hyperchaotic system, the researchers managed to implement an electronic circuit with a relatively straightforward architecture for its realization.

Recently, a new direction in nonlinear circuit theory has been actively developed: chaos generators based on memristors. The term "memristor" was first coined by Chua [17] to describe a device based on the symmetrical principle, in which an electric charge is coupled to a magnetic flux. Essentially, a memristor functions as a resistor with an analog memory. Over time, the term has been extended to encompass a broader category of memristor systems [18]. The initial implementation of a memristor device with a metal-dielectric-metal structure was achieved by the HP laboratory [19]. A comprehensive review of memristive hyperchaotic systems is described in the monograph [20]. There are not many types of memristor-based multidimensional hyperchaotic systems known in the literature. Wang et al. [21] proposed a new 5D chaotic system with a flux-controlled memristor. Mezatio et al. [22] presented a 6D autonomous system obtained by introducing a flux-controlled memristor model into an existing 5D hyperchaotic autonomous system. Kou et al. [23] introduced an unusual 7D complex chaotic system combined with the cubic memristor. Unlike previous studies [21]-[23], we proposed a new 8D hyperchaotic system obtained by introducing a flux-controlled memristor model into a new 7D hyperchaotic system.

The purpose of this paper is to create computer models for new nonlinear dynamic systems (7D and 8D) using both the MATLAB-Simulink environment and LabView software. To test new electronic circuits for chaos generators, we use the NI Multisim package. This package allows users to display chaotic dynamics through signal oscillograms and phase portraits of attractors.

II. EQUATIONS 7D AND 8D OF NONLINEAR DYNAMICS

Recently [10], we carried out a computer simulation of a 6D chaotic system, describing scenarios for the emergence of a turbulent state in a non-uniformly rotating magnetized electrically conducting fluid. This model is described by nonlinear dynamics equations of the following forms [10]:

$$\begin{cases} \frac{dx_1}{dt} = -x_1 + Rx_2 - bx_4 - cx_5 \\ \frac{dx_2}{dt} = c(-x_2 + x_1 - x_1x_3) \\ \frac{dx_3}{dt} = c(-dx_3 + x_1x_2) \\ \frac{dx_4}{dt} = -x_4 + cx_1 \\ \frac{dx_5}{dt} = -x_5 + ex_1 + bx_6 \\ \frac{dx_6}{dt} = -x_6 - fx_4 - cx_5 \end{cases} \quad (1)$$

Here, the amplitudes of velocity field disturbances are represented by x_1 and x_5, while magnetic field disturbances are indicated by x_4 and x_6. Temperature field disturbances, on the other hand, are represented by the amplitudes x_2 and x_3. Parameters R, b, c, d, e and f are all positive real numbers and R is a bifurcation parameter (the Rayleigh number). Varying the values of the parameter R will allow us to consider a one-parameter set of solutions. The physical meaning of R lies in the temperature difference at the boundaries of the electrically conductive liquid layer. By changing the heating conditions at the boundaries of the liquid layer, i.e., value R, one can investigate various regimes of convective instability. When $b = 2, c = 0.1, d = 8/3, e = 8.21, f = 24.65,$ and $R = 58$, the system (1) depicts hyperchaotic behavior with two positive Lyapunov exponents in six Lyapunov exponents as

$L_1 = 0.0988591, L_2 = 0.0109865, L_3 = -0.544226,$

$L_4 = -1.00557, L_5 = -1.15581, L_6 = -1.77091.$

at initial conditions:

$x_1(0) = x_2(0) = x_3(0) = x_4(0) = x_5(0) = x_6(0) = 1.$

The sum of the Lyapunov exponents is negative $\sum_{i=1}^{6} L_i = -4.36667 < 0$, indicating that the hyperchaotic system (1) is dissipative. For a hyperchaotic system (1), the Kaplan-York dimension (KYD) has the following forms:

$$D_{KY} = M + \frac{1}{|L_{M+1}|}\sum_{i=1}^{M} L_i, \quad (2)$$

where M is the largest integer and

$\sum_{i=1}^{M} L_i > 0, \quad \sum_{i=1}^{M+1} L_i < 0.$

The value of the Kaplan-York dimension turns out to be not an integer $D_{KY} = 2 + \frac{L_1 + L_2}{|L_3|} \approx 2.20,$ but a fractional or fractal one. Consequently, this system behaves chaotically. Next, we introduce an additional variable U to improve the chaotic behavior of system (1) by modifying the Lorentz equations included in the system of equations (1). As a result, we obtain a new system of 7D equations for nonlinear dynamics:

$$\begin{cases} \frac{dx_1}{dt} = -x_1 + Rx_2 - 2x_4 - 0.1x_5 - U \\ \frac{dx_2}{dt} = 0.1(-x_2 + x_1 - x_1x_3) \\ \frac{dx_3}{dt} = 0.1(-2.667x_3 + x_1x_2) \\ \frac{dx_4}{dt} = -x_4 + 0.1x_1 \\ \frac{dx_5}{dt} = -x_5 + 8.21x_1 + 2x_6 \\ \frac{dx_6}{dt} = -x_6 - 24.65x_4 - 0.1x_5 \\ \frac{dU}{dt} = -10x_2 - 5.1U \end{cases} \quad (3)$$

By integrating a memristor with a chaotic system (3), a novel 8D chaotic system can be constructed. To facilitate this, we adopted the model of an "absolute memristor" or a magnetically controlled memristor (see, for example, [24]). The mathematical representation of the magnetically controlled memristor is expressed by the following equations [24]:

$$\begin{cases} I = W(\varphi)U \\ \frac{d\varphi}{dt} = U \\ W(\varphi) = \alpha - \beta|\varphi| \end{cases} \quad (4)$$

Here U, I, and φ are the input, output and state of the memristive device, respectively. In equations (4), $W(\varphi)$ represents a function of magnetic flux φ, and α and β are constant coefficients chosen as [23] $\alpha = 1$ and $\beta = 0.1$. The graph of the function for system (4) forms a smooth quadratic nonlinear characteristic curve that passes through the origin. The Simulink circuit for an absolute memristor is depicted in Figure 1.

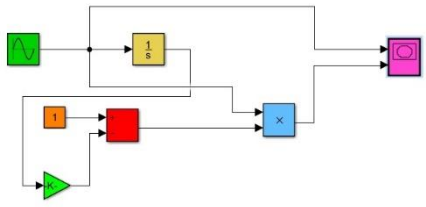

Figure 1: Simulink circuit for modeling an absolute memristor.

The sinusoidal AC voltage source U is the input of the memristor and can be expressed as: $U = A\sin(2\pi ft)$, where A and f are the amplitude and frequency of the external signal, respectively. Figure 2 illustrates the simulation outcomes of the memristor circuit (refer to Figure 1). Under sinusoidal excitation with alternating current, the current-voltage characteristic of the memristor forms a closed curve - a hysteresis loop passing through the origin of coordinates. As the frequency f rises, the area of the hysteresis loop gradually diminishes, and conversely, with an increase in amplitude A, it expands. This behavior aligns with the fundamental properties of memristors.

Applying expressions (4) to the system of 7D nonlinear dynamics equations (3), we obtained new memristor-based 8D nonlinear dynamics equations in the following form:

$$\begin{cases} \frac{dx_1}{dt} = -x_1 + Rx_2 - 2x_4 - 0.1x_5 - W(\varphi)U \\ \frac{dx_2}{dt} = 0.1(-x_2 + x_1 - x_1x_3) \\ \frac{dx_3}{dt} = 0.1(-2.667x_3 + x_1x_2) \\ \frac{dx_4}{dt} = -x_4 + 0.1x_1 \\ \frac{dx_5}{dt} = -x_5 + 8.21x_1 + 2x_6 \\ \frac{dx_6}{dt} = -x_6 - 24.65x_4 - 0.1x_5 \\ \frac{dU}{dt} = -10x_2 - 5.1U \\ \frac{d\varphi}{dt} = U \end{cases} \quad (5)$$

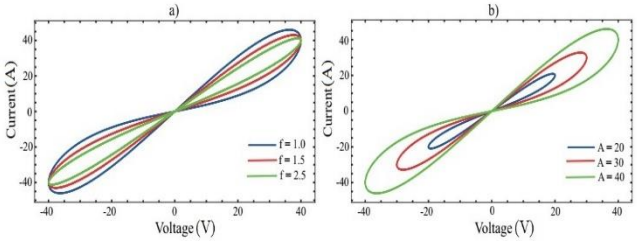

Figure 2: Simulation of the hysteresis loop of an absolute memristor: a) different values of frequency f; b) different amplitude value A.

or in the form of state variables x_i in Eqs. (6), we write as

$$\begin{cases} \frac{dx_1}{dt} = -x_1 + Rx_2 - 2x_4 - 0.1x_5 - (1 - 0.1x_8)x_7 \\ \frac{dx_2}{dt} = 0.1(-x_2 + x_1 - x_1x_3) \\ \frac{dx_3}{dt} = 0.1(-2.667x_3 + x_1x_2) \\ \frac{dx_4}{dt} = -x_4 + 0.1x_1 \\ \frac{dx_5}{dt} = -x_5 + 8.21x_1 + 2x_6 \\ \frac{dx_6}{dt} = -x_6 - 24.65x_4 - 0.1x_5 \\ \frac{dx_7}{dt} = -10x_2 - 5.1x_7 \\ \frac{dx_8}{dt} = x_7 \end{cases} \quad (6)$$

The dynamic behavior of the new systems (3) and (6) presented in this paper is studied in the subsequent sections.

III. ANALYSIS OF THE STABILITY AND DYNAMICS OF A 7D CHAOTIC SYSTEM

In this section, we will describe both qualitative and numerical analyses of the newly introduced nonlinear dynamic system of equations (3).

A. *Bifurcation diagrams, Lyapunov exponents and Kaplan-Yorke dimension*

When examining nonlinear dynamic systems, a common practice involves utilizing a graphical representation, such as a bifurcation diagram, to depict alterations in the state variables of the system. This diagram provides essential information about the qualitative shifts in the system's behavior as certain control parameters vary. Following a similar approach as in reference [20], we designated the parameter R in the system (3) as a controlling factor. In Figure 3, bifurcation diagrams are presented for the $x_1, x_2, x_4, x_5, x_6, x_7$ components of system (3) with respect to variations in R within the interval $R \in [0.600]$. These diagrams enable the identification of stable regions (represented by individual points) or regular behaviors within the system. The diagrams can also reveal areas where the system demonstrates periodic or quasi-periodic behavior. Distinct branches on the diagram may correspond to different periodic orbits, signifying diverse oscillation patterns. In addition, on bifurcation diagrams, one can observe period-doubling bifurcations when the parameter R changes. These bifurcations constitute a sequence wherein

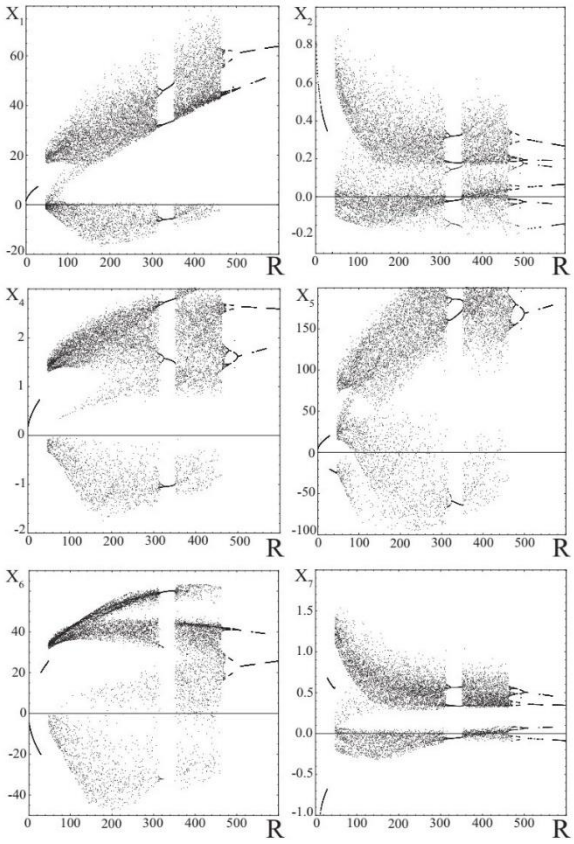

Figure 3: Bifurcation diagrams for $x_1, x_2, x_4, x_5, x_6, x_7$ components of the system (3) depending on changes in the parameter R.

the system transitions from one period to period doubling (doubling of periods), and this process may persist, eventually leading to chaotic behavior. By setting the parameter $R = 68$, we generated a bifurcation diagram while varying the parameter d. As depicted in Figure 4, it is evident that when $d = 8/3 \approx 2.667$ (matching the value in the Lorentz system [4]), chaos is observed in system (3).

An essential criterion for characterizing the chaotic behavior of a nonlinear dynamic system is the Lyapunov spectrum. Lyapunov exponents are employed to determine the rate of convergence or divergence between trajectories in the phase space. The existence of at least one positive value in the Lyapunov spectrum indicates the presence of chaotic vibrations in the system. The number of Lyapunov exponents corresponds to the dimension of the phase space of the nonlinear dynamic system. For our system (4), there are seven such indicators. Following the methodology of Sandri [25] and Binouse et al. [26], we computed the maximum Lyapunov exponent for (3) at $R = 68$: $L_{max} = 0.157485$. Subsequently, employing Gram-Schmidt orthogonalization, all Lyapunov exponents are precisely determined as follows:

$$L_1 = 0.063631, L_2 = 0.0465695, L_3 = -0.507604,$$
$$L_4 = -1.04418, L_5 = -1.13397, \quad (7)$$
$$L_6 = -1.78984, L_7 = -5.10153.$$

It is observed that the Lyapunov spectrum contains two positive Lyapunov exponents, indicating hyperchaotic behavior in the system (3). Additionally, as $L_1 + L_2 + L_3 + L_4 + L_5 + L_6 + L_7 = -9.4669235 < 0$, the new hyperchaotic system (3) is characterized as dissipative. The dimension of the Kaplan-Yorke dimension of the new hyperchaotic system (3) is computed using the formula (2) as follows:

$$D_{KY} = 2 + \frac{L_1 + L_2}{|L_3|} \approx 2.217. \quad (8)$$

Hence, we have determined the Kaplan-Yorke dimension (8) to be slightly higher than that of the 6D chaotic system (1), indicating a greater complexity in the dynamics of the system (3). Figure 5 illustrates the dynamics of the Lyapunov exponents of the hyperchaotic system (3).

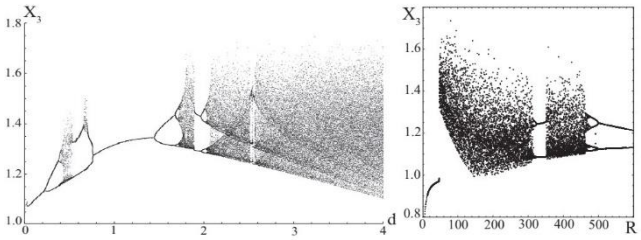

Figure 4: Bifurcation diagrams for the x_3 component of the system (3) depending on changes in the parameters d and R.

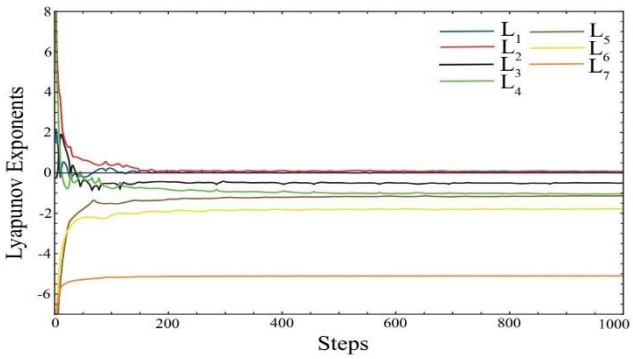

Figure 5: The convergence plot of the Lyapunov spectrum for the system (3).

B. *Stability analysis*

Some of the dynamical properties of the system (3 are explored, as described below.

Symmetry. Because the transformation

$$(x_1, x_2, x_3, x_4, x_5, x_6, x_7) \rightarrow (-x_1, -x_2, x_3, -x_4, -x_5, -x_6, -x_7)$$

does not change the system, it is symmetric about the x_3-axis.

Dissipativity: The divergence of the system can be calculated as $\mathrm{div}\Phi = \sum_{i=1}^{7} \frac{\partial \dot{x}_i}{\partial x_i} = -9.466 < 0.$

Equilibrium points and stability. Setting the left sides of equations (3) to zero, we identified three equilibrium points:

$E_0(0,0,0,0,0,0,0),$

$E_{1,2}(\pm 11.11, \pm 0.234, 0.98, \pm 1.11, \pm 30.336, \mp 30.426, \mp 0.458).$

Linearizing equation (3) around this set of equilibria, we obtained the Jacobian matrix of the system as follows:

$$J(E) = \begin{pmatrix} -1 & 68 & 0 & -2 & -0.1 & 0 & -1 \\ 0.1(1-x_3) & -0.1 & -0.1x_1 & 0 & 0 & 0 & 0 \\ 0.1x_2 & 0.1x_1 & -0.2667 & 0 & 0 & 0 & 0 \\ 0.1 & 0 & 0 & -1 & 0 & 0 & 0 \\ 8.21 & 0 & 0 & 0 & -1 & 2 & 0 \\ 0 & 0 & 0 & -24.65 & -0.1 & -1 & 0 \\ 0 & -10 & 0 & 0 & 0 & 0 & -5.1 \end{pmatrix} \quad (9)$$

The characteristic polynomial at the equilibrium point E_0 is written as

$$P(\lambda) = \lambda^7 + 9.4667\lambda^6 + 24.1846\lambda^5 - 4.2531\lambda^4 - \\ -92.5309\lambda^3 - 133.8202\lambda^2 - -71.2131\lambda - 11.1785 \quad (10)$$

Eigenvalues are obtained as

$\lambda_1 = -5.0299,\ \lambda_2 = 1.9954,\ \lambda_3 = -3.0470,\ \lambda_4 = -1.1497 + i0.5928,$

$\lambda_5 = -1.1497 - i0.5928,\ \lambda_6 = -0.8190,\ \lambda_7 = -0.2667.$

From this, we saw that not all real parts of the eigenvalues are negative. Then, according to the Routh-Hurwitz stability condition, the equilibrium point E_0 is unstable. At the equilibrium point $E_{1,2}$, the characteristic polynomial has the following form:

$$P(\lambda) = \lambda^7 + 9.4667\lambda^6 + 32.0832\lambda^5 + 65.4815\lambda^4 + \\ +97.0256\lambda^3 + 106.6226\lambda^2 + 77.2612\lambda + 22.2727 \quad (11)$$

The eigenvalues are:

$\lambda_1 = -5.0966,\ \lambda_2 = -1.1106 + i1.0009,$

$\lambda_3 = -1.1106 - i1.0009,\ \lambda_4 = -1.6514,$

$\lambda_5 = -0.5828,\ \lambda_6 = 0.0428 + i1.4244,$

$\lambda_7 = 0.0428 - i1.4244.$

As can be seen from equation (11), all coefficients have a positive sign; therefore, according to the Routh-Hurwitz condition, the equilibrium points $E_{1,2}$ are stable.

IV. ANALYSIS OF A NEW MEMRISTOR-BASED HYPERCHAOTIC SYSTEM

In this section, a numerical analysis is presented for a novel 8D hyperchaotic memristor-based system (6) derived from the 7D hyperchaotic system (3).

A. Bifurcation diagrams, Lyapunov exponents and Kaplan-Yorke dimension

By varying the parameter R within the interval $R \in [0, 600]$, we constructed bifurcation diagrams for the components $x_1, x_2, x_4, x_5, x_6, x_7$ of the nonlinear dynamic system (6) incorporating a memristor. These diagrams are illustrated in Figure 6. Upon comparison with the diagrams in Figure 3, it becomes evident that the chaotic behavior is most pronounced in the 8D memristor system. This is further emphasized in Figure 7, where a bifurcation diagram for the x_3 component is plotted for a fixed parameter $R = 68$, showcasing developed chaos at $d = 8/3 \approx 2.667$.

Employing a methodology akin to the previous section, we computed the maximum Lyapunov exponent for (6) at $R = 68$: $L_{max} = 0.18397$. The system (6) is a hyperchaotic system with three positive Lyapunov exponents. All Lyapunov exponents are precisely determined as follows:

$$L_1 = 0.041391, L_2 = 0.0317815, L_3 \approx 0,$$
$$L_4 = -0.408706, L_5 = -1.11737, L_6 = -1.1493, \quad (12)$$
$$L_7 = -1.7399, L_8 = -5.08168.$$

Figure 8 shows the dynamics of the hyperchaotic system's Lyapunov exponents (6). Furthermore, because $L_1 + L_2 + L_3 + L_4 + L_5 + L_6 + L_7 + L_8 = -9.4237835$, the new hyperchaotic system (6) is dissipative. Using definition (2) and expressions (12), we calculated the Kaplan-York dimension:

$$D_{KY} = 3 + \frac{L_1 + L_2 + L_3}{|L_4|} \approx 3.179 \quad (13)$$

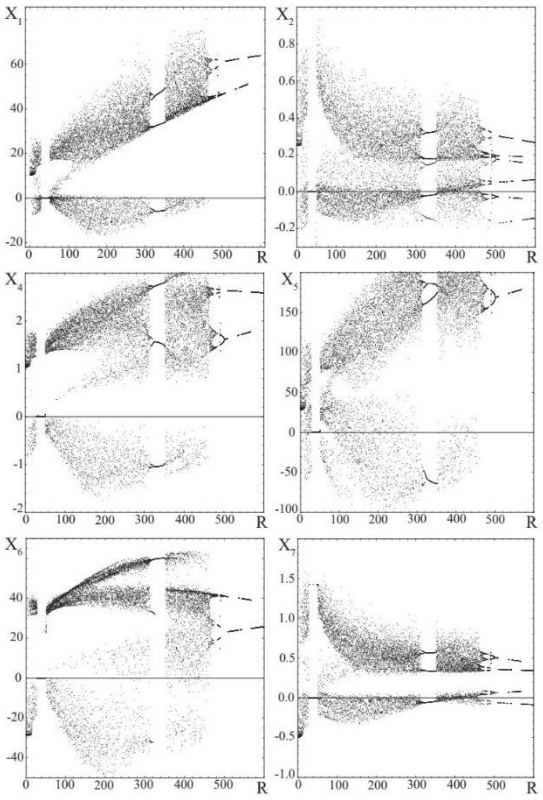

Figure 6: Bifurcation diagrams for $x_1, x_2, x_4, x_5, x_6, x_7$ components of the system (6) depending on changes in the parameter R.

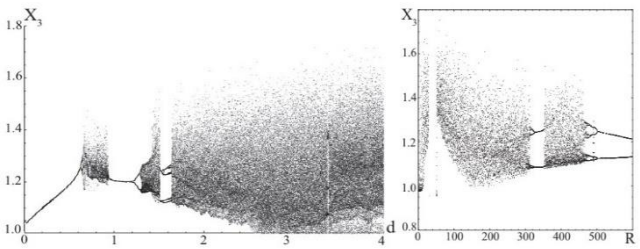

Figure 7: Bifurcation diagrams for the x_3 component of the system (6) depending on changes in the parameters d and R.

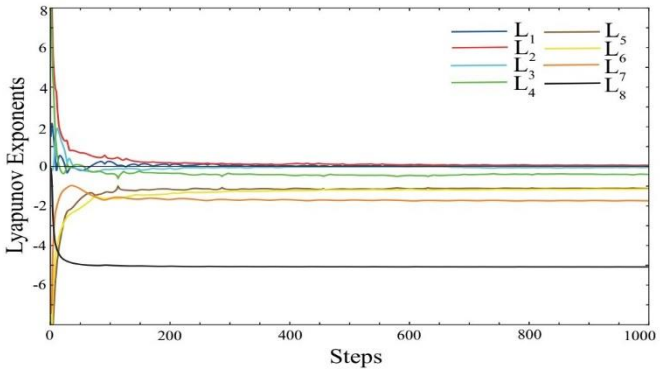

Figure 8: The convergence plot of the Lyapunov spectrum for the system (6).

Hence, we have established that the memristive system (6) possesses a higher Kaplan-York dimension compared to system (3). This implies that system (7) is more chaotic, complex, and potentially exhibits a more intricate fractal structure in its dynamics.

B. Stability analysis

The dynamic properties of system (6) are analyzed as shown below.

Symmetry. Unlike system (3), memristive system (6) is not invariant under the transformation:

$$(x_1, x_2, x_3, x_4, x_5, x_6, x_7, x_8) \rightarrow$$
$$\rightarrow (-x_1, -x_2, x_3, -x_4, -x_5, -x_6, -x_7, -x_8).$$

Dissipativity The divergence of system (6) being less than zero indicates that the system is dissipative, suggesting the possibility of chaotic attractors within the system.

Equilibrium points and stability. By setting the right-hand sides of the equations in system (6) to zero, we can determine equilibrium points, which are located on a line: $E_0(0,0,0,0,0,0,0,\tilde{x}_8)$. Linearizing Eqs. (6) around this set of equilibria, we obtained the Jacobian matrix of the system as follows:

$$J(E) = \begin{vmatrix} -1 & 68 & 0 & -2 & -0.1 & 0 & -1+0.1x_8 & 0.1x_7 \\ 0.1(1-x_3) & -0.1 & -0.1x_1 & & 0 & 0 & 0 & 0 & 0 \\ 0.1x_2 & 0.1x_1 & -0.2667 & & 0 & 0 & 0 & 0 & 0 \\ 0.1 & 0 & 0 & -1 & 0 & 0 & 0 & 0 \\ 8.21 & 0 & 0 & 0 & -1 & -2 & 0 & 0 \\ 0 & 0 & 0 & -24.65 & -0.1 & -1 & 0 & 0 \\ 0 & -10 & 0 & 0 & 0 & 0 & -5.1 & 0 \\ 0 & 0 & 0 & 0 & 0 & 0 & 1 & 0 \end{vmatrix}$$

The characteristic polynomial of the Jacobian matrix can be expressed as follows:

$$P(\lambda) = \lambda^8 + 9.4667\lambda^7 + 24.1846\lambda^6 - 4.2531\lambda^5 - \\ -133.8202\lambda^3 - 92.5309\lambda^4 - 71.2131\lambda^2 - 11.1785\lambda + \\ +0.032\lambda\tilde{x}_8 + 0.4\lambda^3\tilde{x}_8 + 0.2053\lambda^2\tilde{x}_8 + 0.1\lambda^5\tilde{x}_8 + \\ +0.3266\lambda^4\tilde{x}_8 \quad (14)$$

According to the Routh-Hurwitz criterion, the equilibrium points $E_0(0,0,0,0,0,0,0,\tilde{x}_8)$ are unstable.

V. COMPUTER MODELLING AND ELECTRONIC CIRCUIT DESIGN

In this section, computer modeling is implemented for the new 7D and 8D hyperchaotic systems of nonlinear dynamics. Utilizing the visual design environments Simulink and Labview, chaotic oscillation generators were developed for the 7D system (3) and the 8D memristive system (6). Additionally, in the Multisim environment, the circuit realization of both the 7D chaotic system and the 8D memristor chaotic system has been completed.

A. MATLAB-Simulink model

Phase portraits of chaotic attractors for the systems of equations (3) and (6) were obtained through numerical simulation in MATLAB -Simulink. The MATLAB-Simulink model for chaotic oscillation generators in the systems (3) and (6) comprises interconnected blocks for signal amplification, summation, subtraction, multiplication, integration, and recording devices. The gain blocks contain information about the values of fixed parameters in systems (3) and (6). The Constant block holds data on the value of the Rayleigh parameter R. For our simulation in MATLAB-Simulink, we set the parameter value $R = 68$. In Figure 9, a MATLAB-Simulink model diagram for the 7D hyperchaotic system (3) is presented. On the other hand, Figure 10 displays a MATLAB-Simulink model diagram for the 8D hyperchaotic memristor system (7). The results of modeling the systems

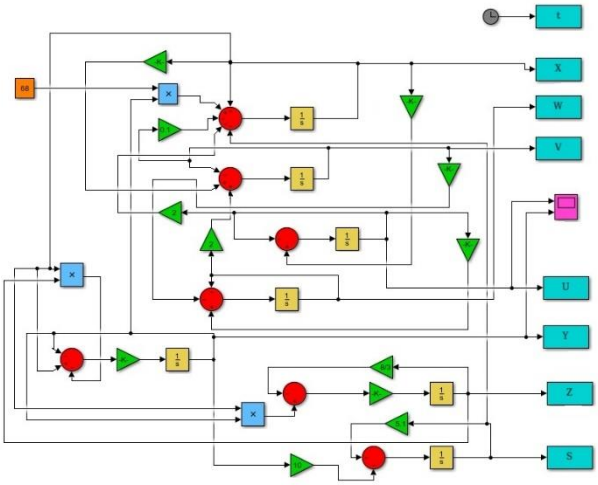

Figure 9: The Matlab-Simulink model for Eq. (3).

1

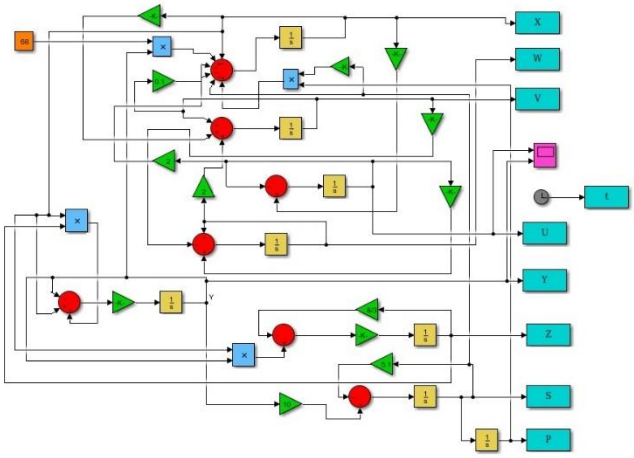

Figure 10: The MATLAB-Simulink model for Eq. (6).2

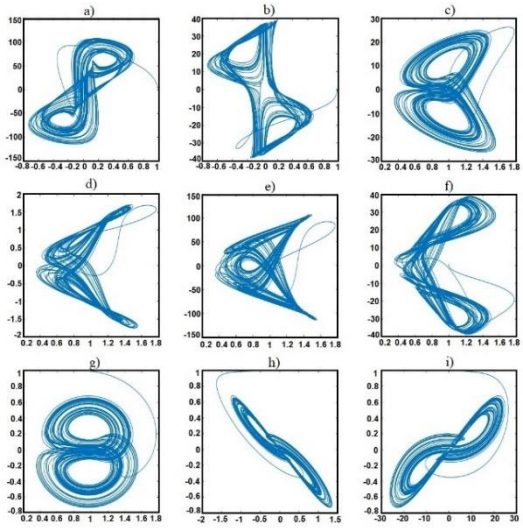

Figure 11: The phase portraits in the planes a) x_2x_5, b) x_2x_6, c) x_3x_1, d) x_3x_4, e) x_3x_5, f) x_3x_6, g) x_3x_2, h) x_7x_2, i) x_1x_2 for system (3).

of equations (3) and (6) with the parameter $R = 68$ are depicted in Figures 11 and 12 respectively. These phase portraits reveal the complexity of trajectories characteristic of strange attractors.

Note that the direct implementation of (3) and (6) using electronic circuits presents a certain difficulty. As seen in Figures 11 and 12, the dynamic variables x_1, x_5, x_6, x_7, x_8 occupy a wide dynamic range with values beyond the reasonable limits of the power supply. The operating voltage range of op-amps in practical electronic circuits is typically -15 V to +15 V.

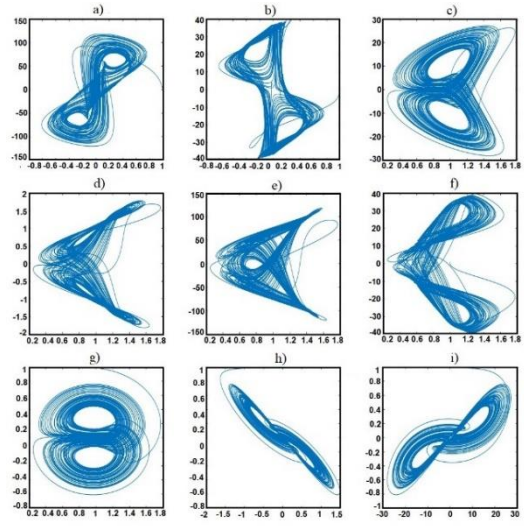

Figure 12: The phase portraits in the planes a) x_2x_5, b) x_2x_6, c) x_3x_1, d) x_3x_4, e) x_3x_5, f) x_3x_6, g) x_3x_2, h) x_7x_2, i) x_1x_2 for system (6).

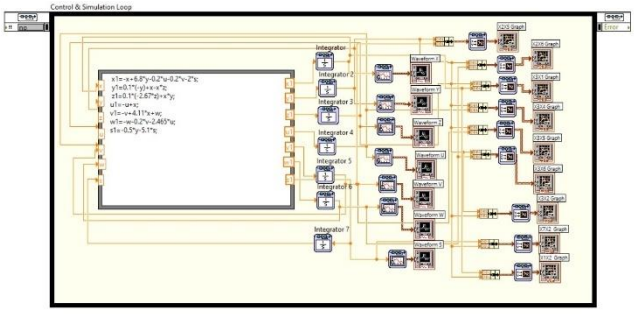

Figure 13: Block diagram implementing a hyperchaotic system (15) in LabVIEW.

This problem can be addressed by transforming the variables in the dynamical systems (3) and (6). In our case, we need to change the scale of the following variables: $x_1 = 10X_1, x_5 = 20X_5, x_6 = 10X_6, x_7 = 20X_6, x_8 = 20X_8$. The remaining variables are simply redesignated as $x_2 = X_2, x_3 = X_3, x_4 = X_4$. With this scaling, the equations (3) are transformed as follows:

$$\begin{cases} \dfrac{dX_1}{dt} = -X_1 + 6.8X_2 - 0.2X_4 - 0.2X_5 - 2X_7 \\ \dfrac{dX_2}{dt} = -0.1X_2 + X_1 - X_1X_3 \\ \dfrac{dX_3}{dt} = -0.267X_3 + X_1X_2 \\ \dfrac{dX_4}{dt} = -X_4 + X_1 \\ \dfrac{dX_5}{dt} = -X_5 + 4.11X_1 + X_6 \\ \dfrac{dX_6}{dt} = -X_6 - 2.465X_4 - 0.2X_5 \\ \dfrac{dX_7}{dt} = -0.5X_2 - 5.1X_7 \end{cases} \tag{15}$$

In a similar way, the memristor-based 8D hyperchaotic system (6) is transformed into the following form:

$$\begin{cases} \dfrac{dX_1}{dt} = -X_1 + 6.8X_2 - 0.2X_4 - 0.2X_5 - 2X_7 + 4X_7X_8 \\ \dfrac{dX_2}{dt} = -0.1X_2 + X_1 - X_1X_3 \\ \dfrac{dX_3}{dt} = -0.267X_3 + X_1X_2 \\ \dfrac{dX_4}{dt} = -X_4 + X_1 \\ \dfrac{dX_5}{dt} = -X_5 + 4.11X_1 + X_6 \\ \dfrac{dX_6}{dt} = -X_6 - 2.465X_4 - 0.2X_5 \\ \dfrac{dX_7}{dt} = -0.5X_2 - 5.1X_7 \\ \dfrac{dX_8}{dt} = X_7 \end{cases} \tag{16}$$

It is important to note that the systems (3) and (15), as well as (6) and (16), are equivalent, since the linear transformation does not change the physical properties of nonlinear systems.

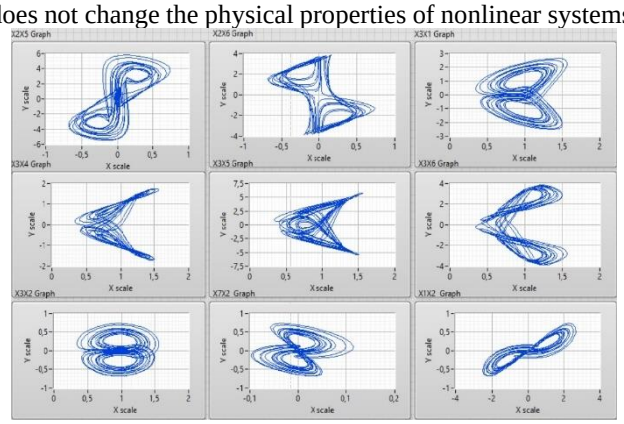

Figure 14: Phase portraits of the rescaled system (15) in various planes obtained in LabVIEW.

B. LabVIEW model

The modeling of nonlinear dynamic systems using various software environments is of significant interest. We employed the LabVIEW software environment to simulate

the behavior of a chaotic system. A visual platform has been created for the development of algorithms in LabVIEW, which is currently widely used in engineering applications [27]. Figure 13 depicts a block diagram of a 7D hyperchaotic system, described by transformed equations (15). Unlike works [10],[12], this model was developed using the Control & Simulation and Formula Node toolkits. The Formula Node is utilized to formulate the right-hand sides of the equations in system (15). Using a Formula Node instead of function blocks results in a simpler block diagram. Integration of time derivatives is performed using Integrator blocks from the Continuous palette.

Figure 14 shows a software interface that illustrates chaotic solutions of transformed equations (15) in a LabVIEW model. The modeling result is displayed as phase portraits in planes:

$X_2X_5, X_2X_6, X_3X_1, X_3X_4, X_3X_5, X_3X_6, X_3X_2, X_7X_2, X_1X_2$

for initial conditions:

$X_1(0) = X_2(0) = X_3(0) = X_4(0) =$

$= X_5(0) = X_6(0) = 1, X_7 = 0.$

It can be seen that the range of values of dynamic variables has decreased significantly compared to the values in Figure 11. This reduction allows the implementation of electronic circuits using operational amplifiers operating in a normal voltage range.

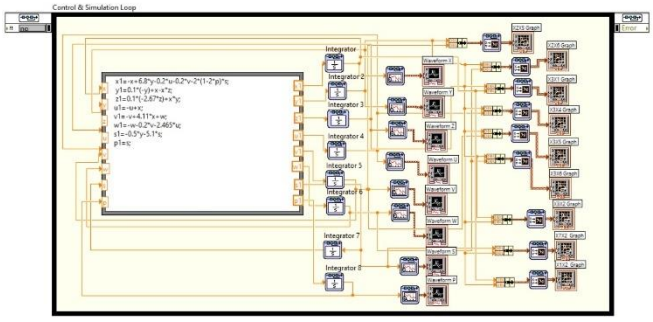

Figure 15: Block diagram implementing a hyperchaotic system (16) in LabVIEW.

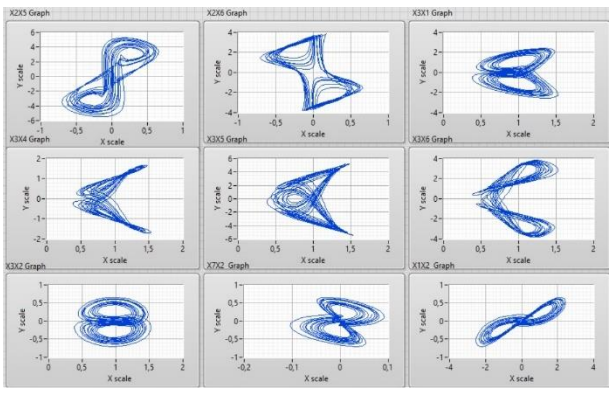

Figure 16: Phase portraits of the rescaled system (16) in various planes obtained in LabVIEW.

Similarly, using Control & Simulation and Formula Node toolkits, we constructed a block diagram of an 8D memristor-based hyperchaotic system, described by transformed equations (16) (see Figure 15). In Figure 16, a software interface is presented that displays the properties of information modeling in the form of phase portraits in the planes

$X_2X_5, X_2X_6, X_3X_1, X_3X_4, X_3X_5, X_3X_6, X_3X_2, X_7X_2, X_1X_2$

for initial conditions:

$X_1(0) = X_2(0) = X_3(0) = X_4(0) =$

$= X_5(0) = X_6(0) = 1, X_7 = X_8 = 0.$

By comparing the phase portraits in Figures 11-12 and 14,16, it is evident that the results of modeling chaotic systems (3) and (7) in MATLAB-Simulink and LabVIEW are consistent.

C. Implementation of new electronic circuits for 7D and memristor-based 8D chaotic systems

To implement the dynamic system of equations (15) in a circuit, seven operational amplifiers are employed to perform the signal integration function. The dynamic system variables (15) are represented by electrical signals corresponding to the instantaneous voltage values on capacitors $C_1, C_2, C_3, C_4, C_5, C_6, C_7$, denoted as $U_1(\tau), U_2(\tau), U_3(\tau), U_4(\tau), U_5(\tau), U_6(\tau), U_7(\tau)$.

Applying Kirchhoff's laws to electrical circuits, we obtain an electrical analog of the system (15):

$$\begin{cases} \frac{dX_1}{dt} = -\frac{10k}{10k}X_1 + \frac{10k}{1.47k}X_2 - \frac{10k}{50k}X_4 - \frac{10k}{50k}X_5 - \frac{10k}{5k}X_7 \\ \frac{dX_2}{dt} = -\frac{10k}{100k}X_2 + \frac{10k}{10k}X_1 - \frac{10k}{1k\cdot 10}X_1X_3 \\ \frac{dX_3}{dt} = -\frac{10k}{37.5k}X_3 + \frac{10k}{1k\cdot 10}X_1X_2 \\ \frac{dX_4}{dt} = -\frac{10k}{10k}X_4 + \frac{10k}{10k}X_1 \\ \frac{dX_5}{dt} = -\frac{10k}{10k}X_5 + \frac{10k}{2.43k}X_1 + \frac{10k}{10k}X_6 \\ \frac{dX_6}{dt} = -\frac{10k}{10k}X_6 - \frac{10k}{4.056k}X_4 - \frac{10k}{50k}X_5 \\ \frac{dX_7}{dt} = -\frac{10k}{20k}X_2 - \frac{10k}{1.96k}X_7 \end{cases} \quad (17)$$

where the output voltages are $X_1, X_2, X_3, X_4, X_5, X_6, X_7$.

The Multisim software environment is employed to devise a circuit capable of generating chaotic oscillations within the system outlined by equations (17). In this procedure, operational amplifiers serve as integrators. The circuit is crafted utilizing conventional methods for integrating, summing, and inverting signals. In Figure 17, the analog circuit depicting system (19) is showcased, wherein the initial three equations are efficiently implemented within a subsystem denoted as SC1. Figure 18 delineates the electronic circuit of the SC1 subsystem (akin to Lorentz equations). The circuits illustrated in Figures 17 and 18 are based on operational amplifiers TL084ACN and analog multipliers A1 and A2. The signal outputs correspond to the labeled terminals in the circuit diagram. By interfacing a dual-channel oscilloscope with different outputs, diverse phase portraits can be derived within the Multisim environment, as exemplified in Figure 19. The results obtained from Multisim outputs closely align with those obtained from MATLAB-Simulink in Figure 11, as well as LabVIEW in Figure 14.

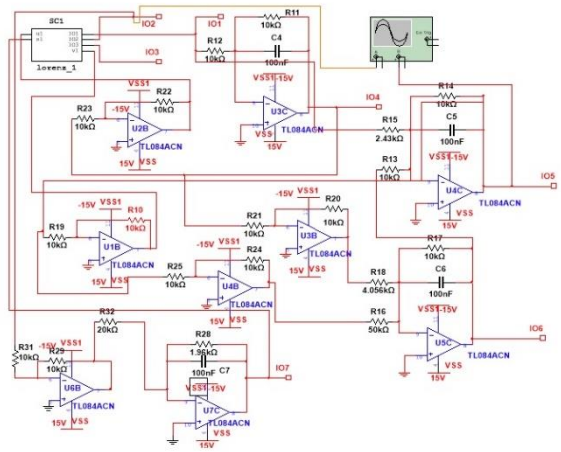

Figure 17: Electronic circuit of the generator of chaotic oscillations based on the system of equations (19).

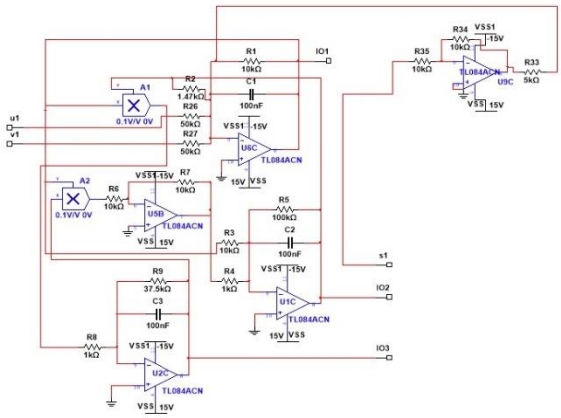

Figure 18: Electronic circuit of the subsystem SC1.

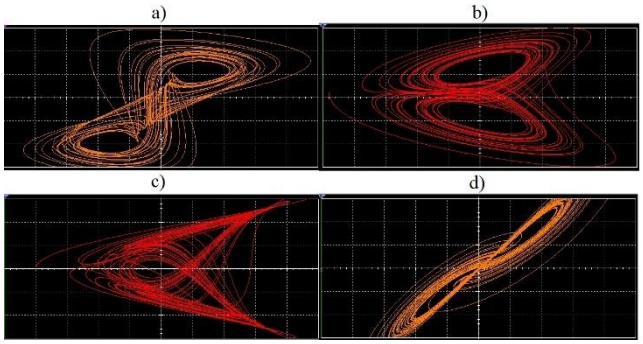

Figure 19: Chaotic phase trajectories displayed in Multisim oscilloscopes: a) X_2X_5 plane with scales 200 mV/div and 2 V/div, b) X_3X_1 plane with scales 200 mV/div and 1 V/div, c) X_3X_5 plane with scales 200 mV/div and 2 V/div, d) X_7X_2 plane with scales 20 mV/div and 200 mV/div.

Utilizing the same approach, we derived the electrical circuit equation corresponding to the dynamic system defined by equations (16):

$$\begin{cases} \frac{dX_1}{dt} = -\frac{10k}{10k}X_1 + \frac{10k}{1.47k}X_2 - \frac{10k}{50k}X_4 - \frac{10k}{50k}X_5 - \frac{10k}{5k}X_7 + \frac{10}{10\cdot 0.250k}X_7X_8 \\ \frac{dX_2}{dt} = -\frac{10k}{100k}X_2 + \frac{10k}{10k}X_1 - \frac{10k}{1k\cdot 10}X_1X_3 \\ \frac{dX_3}{dt} = -\frac{10k}{37.5k}X_3 + \frac{10k}{1k\cdot 10}X_1X_2 \\ \frac{dX_4}{dt} = -\frac{10k}{10k}X_4 + \frac{10k}{10k}X_1 \\ \frac{dX_5}{dt} = -\frac{10k}{10k}X_5 + \frac{10k}{2.43k}X_1 + \frac{10k}{10k}X_6 \\ \frac{dX_6}{dt} = -\frac{10k}{10k}X_6 - \frac{10k}{4.056k}X_4 - \frac{10k}{50k}X_5 \\ \frac{dX_7}{dt} = -\frac{10k}{20k}X_2 - \frac{10k}{1.96k}X_7 \\ \frac{dX_8}{dt} = \frac{10k}{10k}X_7 \end{cases} \quad (18)$$

Figure 20 shows the electronic diagram of the above system of equations, built in the Multisim environment. In this configuration, the SC2 subsystem is employed for convenience, designed specifically for the first three and last equations of the above system of equations. Within the SC2 subsystem, the electronic circuit of the memristor emulator is highlighted with a thick line. The electronic circuit of the SC2 subsystem is detailed in Figure 21. Observing Figure 20 and Figure 21, it becomes apparent that the circuits are also constructed based on operational amplifiers TL084ACN and analog multipliers A1, A2, and A3 (typically, multipliers of the AD633 series are commonly used in practice). The terminals IO1, IO2, IO3, IO4, IO5, IO6, IO7 on the diagram (Figure 20) correspond to signal outputs $X_1, X_2, X_3, X_4, X_5, X_6, X_7$. By connecting a two-channel oscilloscope to different terminals, various phase portraits can be obtained in the Multisim environment, as illustrated in Figure 22. Notably, the simulation results in Multisim demonstrate a commendable agreement with the simulation results in MATLAB-Simulink and LabView, as presented in Figure 12 and Figure 16.

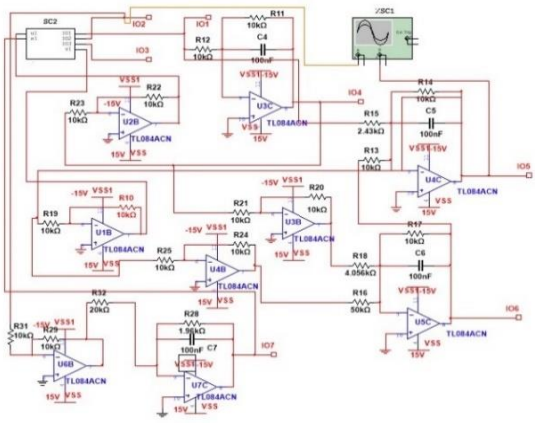

Figure 20: Electronic circuit of the generator of chaotic oscillations based on the system of equations (20).

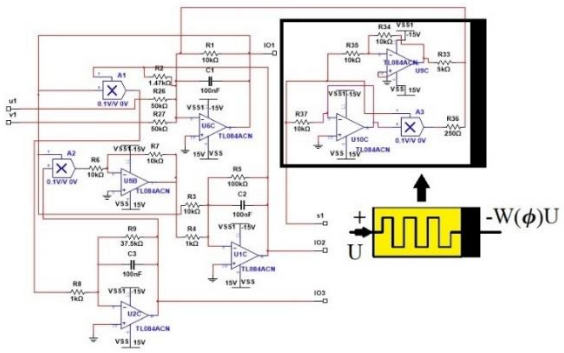

Figure 21: The electronic circuit of the SC2 subsystem containing the memristor emulator circuit.

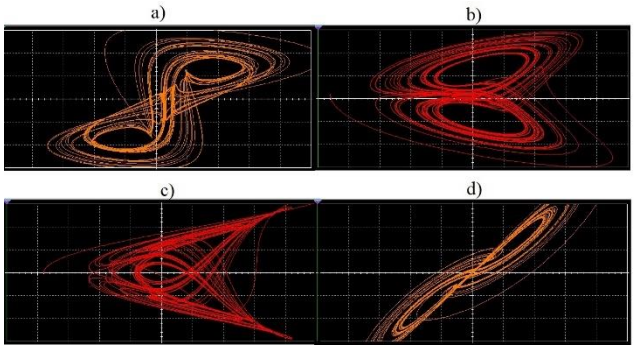

Figure 22: Chaotic phase trajectories of a memristor electronic circuit displayed in Multisim oscilloscopes: a) X_2X_5 plane with scales 200 mV/div and 2 V/div, b) X_3X_1 plane with scales 200 mV/div and 1 V/div, c) X_3X_5 plane with scales 200 mV/div and 2 V/div, d) X_7X_2 plane with scales 20 mV/div and 200 mV/div.

VI. CONCLUSION

This study introduces two novel hyperchaotic systems with dimensions of seven and eight, respectively. Within the 7D system, three equilibrium points exist, with one being unstable and the others stable. Notably, the new 7D system demonstrates heightened chaotic behavior compared to the 6D system, a conclusion supported by the Kaplan-York dimension. In an effort to augment chaos, a "memristor" was incorporated into the equations governing the 7D nonlinear dynamics, resulting in the derivation of a new eight-dimensional (8D) nonlinear system of equations. Remarkably, the Kaplan-York dimension for the 8D system proved to be significantly higher than that of the 7D system, indicating an amplified level of chaos. The newly developed 8D hyperchaotic memristive system exhibits an infinite number of equilibrium points are present, all situated along a line. Bifurcation diagrams for both the 7D and 8D systems illustrate various modes of behavior, encompassing periodic, quasiperiodic, and chaotic patterns. To study the dynamics of these new systems, comprehensive numerical simulations were conducted utilizing MATLAB-Simulink and LabView models. The simulations unveiled intricate chaotic oscillations in the novel systems, with the memristive system displaying particularly complex behavior, evident in the phase portraits. Thus, the new 8D hyperchaotic system may generate multiple attractors with high fractal dimensions. Furthermore, electronic circuits for generating chaos in both the 7D and 8D systems were conceived using operational amplifiers. These circuits were subsequently designed and tested within the Multisim environment. The future direction of this work entails hardware implementations of the newly developed systems, coupled with their practical applications.

ACKNOWLEDGMENT

The author is grateful to the anonymous reviewers for their valuable comments and interest in the manuscript.

REFERENCES

[1] K. Benkouider, M. Halimi, T. Bouden, "Secure communication scheme using chaotic time-varying delayed system," Int. J. Comput. Appl. Technol., vol. 60(2), pp. 175-182, 2019.

[2] Fei Yu, Zinan Zhang, Li Li, Hui Shen, et al. "Secure communication scheme based on a new 5d multistable four-wing memristive hyperchaotic system with disturbance inputs," Complexity, vol. 2020, pp. 1-16, 2020.

[3] S. A. Gebereselassie, B. K. Roy, "A new secure speech communication scheme based on hyperchaotic masking and modulation," IFAC-PapersOnLine, vol. 55, pp. 914-919, 2022.

[4] E. N. Lorenz, "Deterministic non-periodic flow," Journal of the Atmospheric Sciences, vol. 20, pp. 130-142, 1963.

[5] K. M. Cuomo, A. V. Oppenheim, "Circuit implementation of synchronized chaos with applications to communications," Physical Review Letters, vol. 71, no. 1, pp. 65-68, Aug. 1993.

[6] C. Yang, W. Zhu, G. Ren, "Approximate and efficient calculation of dominant Lyapunov exponents of high-dimensional nonlinear dynamic systems," Commun. Nonlinear Sci. Numer. Simul., vol. 18, pp. 3271-3277, 2013.

[7] S. Vaidyanathan, S. He, A. Sambas, "A new multistable double-scroll 4-D hyperchaotic system with no equilibrium point, its bifurcation analysis, synchronization and circuit design," Archives of Control Sciences, vol. 31(1), pp. 99-128, 2021.

[8] J. P. Singh, K. Rajagopal, B. K. Roy, "A new 5D hyperchaotic system with stable equilibrium point, transient chaotic behaviour and its fractional-order form," Pramana, 2018, vol. 91(3), pp. 1-10. 2018

[9] K. A. Alattas, J. Mostafaee, A. Sambas, A. K. Alanazi, S. Mobayen, A. Zhilenkov, "nonsingular integral-type dynamic finite-time synchronization for hyper-chaotic systems," Mathematics, vol. 10(1), pp. 115-136. 2022.

[10] M. Kopp and A. Kopp, "A new 6d chaotic generator: computer modelling and circuit design," Int. J. Eng. Technol., vol.12, pp. 288-307, 2022.

[11] S. N. Lagmiri, M. Amghar, N. Sbiti, "Seven dimensional new hyperchatic systems: dynamics and synchronization by a high gain observer design," Int J. Control and Automation, 2017, vol. 10, no.1,pp. 251-266. 2017.

[12] M. Kopp, A. Kopp, "A new 8d lorenz-like hyperchaotic system: computer modelling, circuit design and arduino uno board implementation," J. Telecommun. Electron. Comput. Eng, vol. 15, no. 2, pp. 37-46, 2023.

[13] J. L. Zhu, J. Dong, H. Q. Gao. "Nine-dimensional eight-order chaotic system and its circuit implementation," Applied Mechanics and Materials, vol. 716-717, pp. 1346-1351, 2014.

[14] E. E. Mahmoud, M. Higazy, T. M. Al-Harthi, "A new nine-dimensional chaotic lorenz system with quaternion variables: complicated dynamics, electronic circuit design, anti-anticipating synchronization, and chaotic masking communication application," Mathematics, vol. 7, no. 10, pp. 877-903, 2019.

[15] Z. Jianliang, K. Shouqiang, G. Huaqiang, W. Yujing, "Ten-dimensional nine-order chaotic system and its circuit implementation," in 2015 IEEE 12th International Conference on Electronic Measurement and Instruments, ICEMI 2015. Institute of Electrical and Electronics Engineers Inc. 2015, 964-968.

[16] K. Benkouider, T. Bouden, A. Sambas, B. Lekouaghet, M. A. Mohamed, S. I. Mohammed, et al., "A new 10D hyperchaotic system with coexisting attractors and high fractal dimension: Its dynamical analysis, synchronization and circuit design," PLoS ONE, vol. 17, no. 4, e0266053, 2022.

[17] L. O. Chua, "Memristor-the missing circuit element," IEEE Transactions on Circuit Theory, vol. 18, no. 5, pp. 507-519, 1971.

[18] L. O. Chua, S. M. Kang, "Memristive Devices and Systems," Proc. IEEE, vol. 64, no. 2, pp. 209-223, 1976.

[19] D. B. Strukov, G. S. Snider, D. R. Stewart, and R. S. Williams, "The missing memristor found," Nature, vol. 453, pp. 80-83, 2008.

[20] V. Sundarapandian, Ch. Volos, Advances in memristors, memristive devices and systems. Springer, Cham, Switzerland, 2017.

[21] R. Wang, M. Li, Z. Gao, and H. Sun, "A New Memristor-Based 5D Chaotic System and Circuit Implementation," Complexity, vol. 2018, Article ID 6069401, 12 p., 2018.
[22] B. A. Mezatio, M. T. Motchongom, B. R. W. Tekam, R. Kengne, R. Tchitnga, A. Fomethe, "A novel memristive 6D hyperchaotic autonomous system with hidden extreme multistability," Chaos, Solitons & Fractals, vol. 120, pp. 100-115, 2019.
[23] L. Kou, Z. Huang, C. Jiang, F. Zhang, W. Ke, J. Wan, H. Liu, H. Li, and J. Lu, "Data encryption based on 7D complex chaotic system with cubic memristor for smart grid," Front. Energy Res., vol. 10, 980863, 2022.
[24] J. Liu, Z. Wang, H. Tian, and F. Xie, "Complex Dynamic Analysis, Circuit Design and Simplified Predefined Time Synchronization for a Jerk Absolute Memristor Chaotic System," Complexity, vol. 2023, Article ID 5912191, 22 p., 2023.
[25] M. Sandri, "Numerical Calculation of Lyapunov Exponents," The Mathematica Journal, vol. 6, pp. 78-84, January 1996.
[26] H. Binous, N. Zakia, "An Improved Method for Lyapunov Exponents Computation,"2008,https://library.wolfram.com/infocenter/MathSource/7109/
[27] R. W. Larsen, "LabVIEW for Engineers". Upper Saddle River: Prentice Hall, 2011.